# A Numerically Efficient Method for the Hydrodynamic Density-Gradient Model

Seonghoon Jin, Young June Park, and Hong Shick Min
School of Electrical Engineering and Computer Science, Seoul National University, Kwanak-Gu, Seoul 151-744, Korea
E-mail : sjin@isis.snu.ac.kr, Tel : +82-2-880-7285, FAX : +82-2-882-4658

***Abstract*— We propose a quantum transport model that is a hydrodynamic extension of the density-gradient model. The governing equations are derived from the moments of the Wigner distribution function and their forms are suitable for the conventional device simulation program. The model is discretized by the control volume method with nonlinear discretizations for the electron and energy flux equations. We also developed a boundary condition for the $\mathrm{Si}/\mathrm{SiO_2}$ interface that includes the electron wavefunction penetration into the oxide to obtain more accurate $C$-$V$ characteristics. As an application, we studied a 25nm NMOSFET device. Compared with the semiclassical models, the new model predicts reduced gate capacitance about 20% and increased subthreshold slope and DIBL about 16% and 46% respectively. Compared with the density-gradient model, the on-current is increased up to 26% due to the nonlocal transport effect.**

## I. Introduction

As the semiconductor device size is scaled down aggressively, its characteristics are changed by the emerging quantum effect. Therefore, semiclassical transport models such as the drift-diffusion (DD) model [1] or the hydrodynamic (HD) model [2] cannot be applied directly to the simulation of nanoscale devices. To overcome this limit of the semiclassical models, various quantum corrected transport models have been proposed [3]–[5]. Among them, the density-gradient (DG) model extends the DD model by including an effective quantum potential in the drift term and it has become one of the successful models that can simulate the quantum effect [3], [6]–[11].

As the magnitude and variation of the electric field increase in the modern devices, hydrodynamic extension of the DG model becomes necessary to include the nonlocal transport effect in addition to the quantum effect.

In the present paper, we will introduce a quantum transport model called *hydrodynamic density-gradient (HDG) model* that extends the DG model by including the energy balance equation. We will describe its governing equations, derivation, boundary conditions, and implementation in detail. As an application, we will discuss the simulation results of a 25nm NMOSFET device.

## II. Basic Models

For simplicity, we consider only the case of electrons. The DG model introduces a nonlocal quantum potential, which depends on the gradient of the electron density as [6]

$$\psi_{\mathrm{qn}} = 2b_{\mathrm{n}}\frac{\nabla^2\sqrt{n}}{\sqrt{n}}, \tag{1}$$

where $n$ is the electron density and $b_{\mathrm{n}} = \hbar^2/\left(12qm_{\mathrm{n}}^{\mathrm{DG}}\right)$ ($m_{\mathrm{n}}^{\mathrm{DG}} = 0.258m_0$ for silicon [7]) is the linear gradient coefficient that represents the strength of the quantum correction.

### A. Governing Equations

In the steady-state condition, our HDG model solves the following set of governing equations:

$$-\nabla\cdot(\epsilon\nabla\psi) - q(p - n + N_{\mathrm{D}}^{+} - N_{\mathrm{A}}^{-}) = 0, \tag{2}$$

$$\nabla\cdot\mathbf{F}_{\mathrm{n}} + U = 0, \tag{3}$$

$$\nabla\cdot\left(b_{\mathrm{n}}\nabla\sqrt{n}\right) - \frac{\sqrt{n}}{2}\psi_{\mathrm{qn}} = 0, \tag{4}$$

and

$$\nabla\cdot\mathbf{S}_{\mathrm{n}} - q\nabla\left(\psi + \frac{5}{2}\psi_{\mathrm{qn}}\right)\cdot\mathbf{F}_{\mathrm{n}} + Uw_{\mathrm{n}} + n\frac{w_{\mathrm{n}} - w_0}{\tau_{\mathrm{wn}}} = 0 \tag{5}$$

with auxiliary equations for the electron and energy fluxes:

$$\mathbf{F}_{\mathrm{n}} = \mu_{\mathrm{n}}n\nabla\left(\psi + \psi_{\mathrm{qn}}\right) - \mu_{\mathrm{n}}\nabla\left(\frac{k_{\mathrm{B}}T_{\mathrm{n}}}{q}n\right) \tag{6}$$

and

$$\mathbf{S}_{\mathrm{n}} = -\kappa_{\mathrm{n}}\nabla T_{\mathrm{n}} + \left(w_{\mathrm{n}} + k_{\mathrm{B}}T_{\mathrm{n}}\right)\mathbf{F}_{\mathrm{n}}, \tag{7}$$

where (2) is the Poisson equation, (3) is the continuity equation, (4) is the quantum potential equation, and (5) is the energy-balance equation. In the above equations, $\epsilon$ is the electric permittivity, $\psi$ is the electrostatic potential, $p$ is the hole density, $T_{\mathrm{n}}$ is the electron temperature, $N_{\mathrm{D}}^{+}$ and $N_{\mathrm{A}}^{-}$ are the ionized donor and acceptor densities, $U$ is the net recombination rate [8], $w_{\mathrm{n}} = \frac{3}{2}k_{\mathrm{B}}T_{\mathrm{n}}$ is the average electron energy (kinetic energy is neglected), $w_0 = \frac{3}{2}k_{\mathrm{B}}T_0$ is the electron energy in equilibrium, $T_0$ is the lattice temperature, $\tau_{\mathrm{wn}}$ is the energy relaxation time, $\mu_{\mathrm{n}}$ is the electron mobility, and $\kappa_{\mathrm{n}} = (5/2 + c)\frac{{k_{\mathrm{B}}}^2}{q}T_{\mathrm{n}}\mu_{\mathrm{n}}n$ ($c = -1.9$) is the thermal conductivity [2]. The unknown variables are $\psi$, $\psi_{\mathrm{qn}}$, $\sqrt{n}$, and $T_{\mathrm{n}}$ for (2), (3), (4), and (5) respectively.

In the derivation of the governing equations from the quantum moment equations [5], we neglect the $\mathbf{v}\cdot\nabla\mathbf{v}$ term in the momentum balance equation and the kinetic energy term ($\frac{1}{2}m_{\mathrm{n}}v^2$) in the energy balance equation. The relation as

$$\nabla\left(nb_{\mathrm{n}}\nabla^2\ln n\right) = n\nabla\left(2b_{\mathrm{n}}\frac{\nabla^2\sqrt{n}}{\sqrt{n}}\right) \tag{8}$$

is used to transform the quantum correction term from the temperature part to the external potential part in (5), (6),


0-7803-7826-1/03/$17.00 © 2003 IEEE

and (7). Compared with [5], our formulation includes the heat flow term ($-\kappa_{\rm n}\nabla T_{\rm n}$) in the energy flux equation and the recombination term ($Uw_{\rm n}$) in the continuity and energy balance equations. As a result, our HDG model exactly returns to the conventional HD model in the classical limit ($b_{\rm n} \to 0$) and the DG model in thermal equilibrium ($T_{\rm n} \to T_0$).

### B. Boundary Conditions

There exist three kinds of boundaries in the simulation domain: electrodes, $\rm Si/SiO_2$ interfaces, and artificial boundaries with the Neumann boundary conditions for fluxes [1].

We apply the Dirichlet boundary conditions at the electrodes by the following assumptions: the electrostatic potential is given as a bias condition, the charge neutrality condition holds, the quantum potential vanishes, and the electrons are in thermal equilibrium ($T_{\rm n} = T_0$).

At the $\rm Si/SiO_2$ interfaces, we can assume that the dielectric flux is continuous and the normal components of the electron and energy fluxes are zero for (2), (3), and (5). For (4), conventional DG model usually sets vanishingly small electron density at the interface by assuming infinite $\rm Si/SiO_2$ potential barrier [9]. But this insulating boundary condition overestimates the quantum confinement effect since the actual potential barrier is finite and the electron wavefunction can penetrate into the oxide. So we propose a new boundary condition for (4).

The electron density penetrated into the oxide by $x$ from the $\rm Si/SiO_2$ interface can be approximated as

$$n(x) = n_0 \exp\left(-2x/x_{\rm np}\right), \tag{9}$$

where $n_0$ is the electron density at the interface and

$$x_{\rm np} = \frac{\hbar}{\sqrt{2m_{\rm nox}\Phi_{\rm Bn}}} = 1.7529\text{Å} \tag{10}$$

is the characteristic penetration depth obtained from the WKB approximation. Here $m_{\rm nox}$ ($0.4m_0$) is the electron effective mass in the oxide and $\Phi_{\rm Bn}$ (3.1 eV) is the potential barrier height [12]. From (9), the outward normal component of the $b_{\rm nox}\nabla\sqrt{n}$ at the interface can be written as

$$\mathbf{n}\cdot b_{\rm nox}\nabla\sqrt{n} = -\left(b_{\rm nox}/x_{\rm np}\right)\sqrt{n_0}, \tag{11}$$

where $b_{\rm nox} = \hbar^2/\left(12qm_{\rm nox}^{\rm DG}\right)$ ($m_{\rm nox}^{\rm DG} = 0.14m_0$) is the linear gradient coefficient for the oxide region. This equation is used as the penetrating boundary condition for (4).

### C. Physical Parameters

The simulation results largely depend on the electron mobility and the energy relaxation time. For the low field mobility ($\mu_{\rm n0}$) model, we apply a local mobility model that includes the lattice scattering, Coulomb scattering with screening effect, surface phonon scattering, and surface roughness scattering [13]. As for the temperature dependent mobility model, we apply the Caughey-Thomas expression with the effective field approach as [14]

$$\mu_{\rm n}\left(T_{\rm n}\right) = \frac{\mu_{\rm n0}}{\left[1+\left\{\frac{3k_{\rm B}\mu_{\rm n0}(T_{\rm n}-T_0)}{2q{v_{\rm satn}}^2\tau_{\rm wn}}\right\}^{\beta}\right]^{1/\beta}}, \tag{12}$$

where $\beta = 2$ and $v_{\rm satn}$ is assumed to be $8\times10^6\,\rm cm/sec$ in the inversion layer.

The energy relaxation time depends on the low field mobility and the electron temperature. An analytic expression for the energy relaxation time can be written as [15]

$$\tau_{\rm wn} = \frac{3}{2}\frac{k_{\rm B}\mu_{\rm n0}}{q{v_{\rm satn}}^2}\frac{T_{\rm n}T_0}{T_{\rm n}+T_0}. \tag{13}$$

Since our sample device has very high channel doping and thin gate oxide, the low field mobility is in the range from 100 to 150 $\rm cm^2/V\cdot sec$. If we assume $\mu_{\rm n0} = 130\,\rm cm^2/V\cdot sec$, the energy relaxation time is in the range from 0.04 to 0.08 psec. Based on this estimation, $\tau_{\rm wn}$ is set to be 0.05 psec.

## III. Numerical Methods

The governing equations are discretized by the control volume method. The flux terms in (2) and (4) are discretized by the central difference scheme. To discretize the electron and energy flux equations, we apply the nonlinear discretization scheme of the HD model [2] by replacing $\psi$ with $\psi+\psi_{\rm qn}$. The discretized form of the electron flux along the mesh line between the ith and jth nodes can be written as

$$F_{\rm n} = -D_{\rm n}\frac{\Delta T}{\Delta x\ln\left(T_{\rm j}/T_{\rm i}\right)}\left[B(\tilde{\Delta})\frac{n_{\rm j}}{T_{\rm j}} - B(-\tilde{\Delta})\frac{n_{\rm i}}{T_{\rm i}}\right], \tag{14}$$

where $\Delta x = x_{\rm j}-x_{\rm i}$, $\Delta T = T_{\rm j}-T_{\rm i}$, $B(x)$ is the Bernoulli function, and

$$\tilde{\Delta} = \frac{\ln\left(T_{\rm j}/T_{\rm i}\right)}{\Delta T}\left[\frac{q}{k_{\rm B}}(\Delta\psi+\Delta\psi_{\rm qn}) - 2\Delta T\right]. \tag{15}$$

Similarly, the discretized form of the energy flux equation can be written as

$$S_{\rm n} = -(5/2+c)\frac{k_{\rm B}D_{\rm n}}{\Delta x}\tilde{N}\left[B(\Phi)T_{\rm j} - B(-\Phi)T_{\rm i}\right], \tag{16}$$

where

$$\tilde{N} = \frac{\Delta T}{\ln\left(T_{\rm j}/T_{\rm i}\right)}\frac{n_{\rm j}}{T_{\rm j}}\frac{B(\tilde{\Delta})}{B(\tilde{\Phi})}, \tag{17}$$

$$\tilde{\Phi} = \frac{\ln\left(T_{\rm j}/T_{\rm i}\right)}{\Delta T}\left[\frac{q}{k_{\rm B}}(\Delta\psi+\Delta\psi_{\rm qn}) - \Delta T\right] - \ln\frac{n_{\rm j}}{n_{\rm i}}, \tag{18}$$

and

$$\Phi = \frac{5/2}{5/2+c}\tilde{\Phi}. \tag{19}$$

The discretized coupled equations are solved by the full Newton method. We found that either iterative or direct matrix solver can be applied. To implement the model, we developed a device simulator called *NANOCAD*.

## IV. Simulation Results and Discussion

We simulated a bulk NMOSFET whose effective channel length is 25 nm and physical oxide thickness is 15Å [16]. The gate material is uniformly doped ($5\times10^{20}\,/\rm cm^3$) $n^+$polysilicon and the channel doping profile is based on the super-halo [17] to prevent the short-channel effect. Fig. 1 shows the doping profile of the device. From this figure, we can find that the source/drain junction depth is 25 nm and the metallurgical channel length is 22 nm [18].


0-7803-7826-1/03/$17.00 © 2003 IEEE

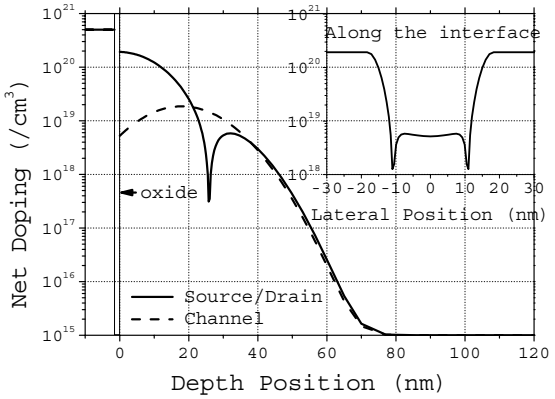


Fig. 1. Doping profile of the 25nm NMOSFET under consideration.

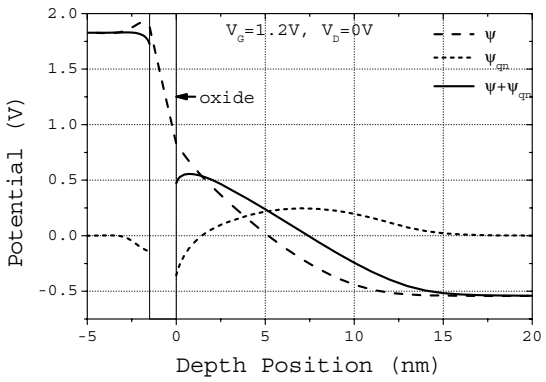


Fig. 3. Comparison of the electrostatic, quantum, and effective potentials along the 1D cut line through the center of the channel.

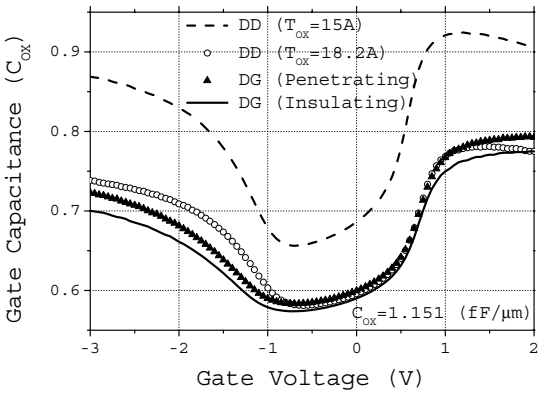


Fig. 2. Comparison of the $C_{\rm G}$-$V_{\rm G}$ characteristics between the DD model ($t_{\rm ox} = 15$Å and $t_{\rm ox} = 18.2$Å) and the DG model (the penetrating boundary condition and the insulating boundary condition).

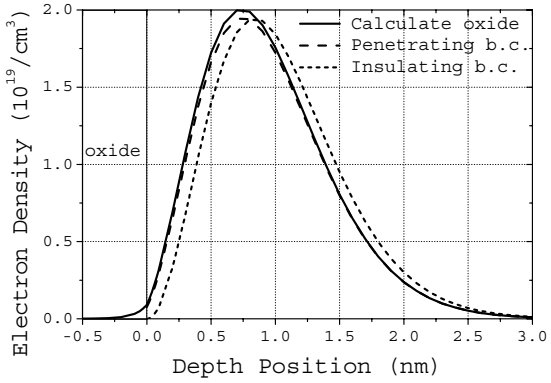


Fig. 4. Comparison of the electron density in the inversion layer.

We first studied the influence of the quantum effect on the gate capacitance. Fig. 2 shows the $C_{\rm G}$-$V_{\rm G}$ characteristics of the device. The quantum effect reduces the gate capacitance about 20% and increases the effective oxide thickness about 3.2Å. Fig. 3 shows the electrostatic, quantum, and effective potentials along the 1D cut line through the center of the channel. The quantum potential smoothes the potential variation near the $\rm Si/SiO_2$ interface. The interface boundary condition also changes the gate capacitance. The penetrating boundary condition increases the gate capacitance slightly compared with the insulating boundary condition. To see the influence of the interface boundary condition, we plotted the electron density in the inversion layer in Fig. 4. As a reference, we calculated the electron density in the oxide as well as in the inversion layer by treating the oxide region as a wide bandgap semiconductor (solid line). The electron density calculated from the penetrating boundary condition follows the solid line very well, while the insulating boundary condition shifts the electron density away from the interface about 1Å.

In Fig. 5, we compared the $I_{\rm D}$-$V_{\rm G}$ characteristics between the HD and HDG models. As we include the quantum effect, the subthreshold slope and DIBL are increased from $93\,\rm mV/dec$ to $108\,\rm mV/dec$ and from $99\,\rm mV$ to $145\,\rm mV$ respectively. Since the quantum confinement effect increases the effective oxide thickness, the gate electrode cannot control the channel charge effectively, which results in the degradation of the short-channel effect.

Fig. 6 shows the $I_{\rm D}$-$V_{\rm D}$ characteristics calculated from the DG and HDG models. The HDG model predicts higher on-current up to 26%, which can be explained by the nonlocal transport effect. Fig. 7 shows the electron temperature in the channel when the bias conditions are in the linear and saturation regions. The electron temperature does not change appreciably until the channel position is about $-10\,\rm nm$, which means that the mobility at the source side of the channel remains high. Fig. 8 shows the average electron velocity in the channel calculated from the DG and HDG models. The HDG model predicts larger electron velocity in the channel, which results in larger on-current. The figure also shows the velocity overshoot effect in the drain side of the channel.

## V. Conclusion

We obtained the HDG model from the quantum moment equations. The HDG model can be viewed as a hydrodynamic extension of the DG model and it returns to the HD model in the classical limit and the DG model in thermal equilibrium. We also improved the boundary condition for the $\rm Si/SiO_2$ interface by including the electron wavefunction penetration


0-7803-7826-1/03/$17.00 © 2003 IEEE

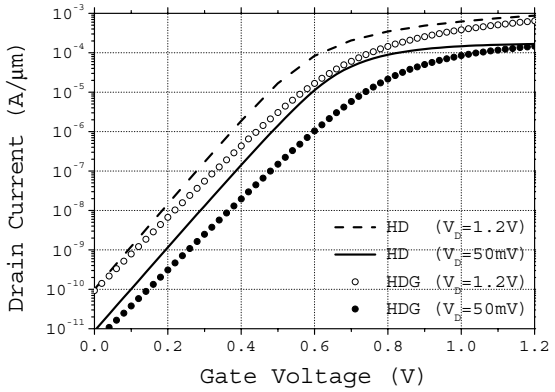


Fig. 5. Comparison of the $I_{\mathrm{D}}$-$V_{\mathrm{G}}$ characteristics of the MOSFET between the HD and HDG models when $V_{\mathrm{D}}$ is $50\,\mathrm{mV}$ and $1.2\,\mathrm{V}$.

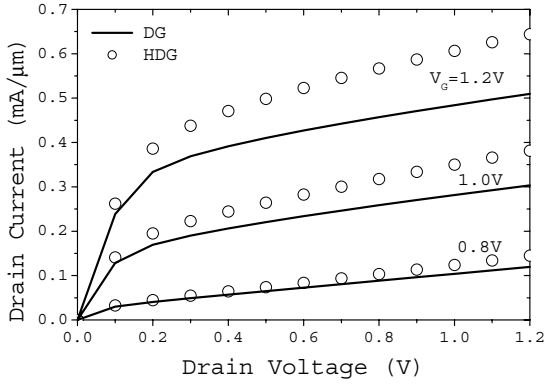


Fig. 6. Comparison of the $I_{\mathrm{D}}$-$V_{\mathrm{D}}$ characteristics between the DG and HDG models when $V_{\mathrm{G}}$ is 0.8, 1.0, and 1.2V.

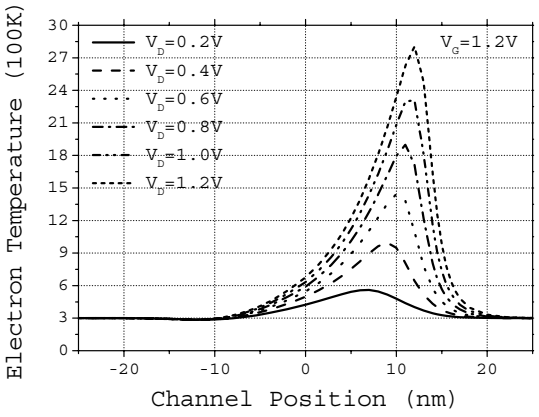


Fig. 7. Electron temperature in the channel when $V_{\mathrm{G}}$ is $1.2V$ and $V_{\mathrm{D}}$ is 0.2, 0.4, 0.6, 0.8, 1.0, and 1.2V.

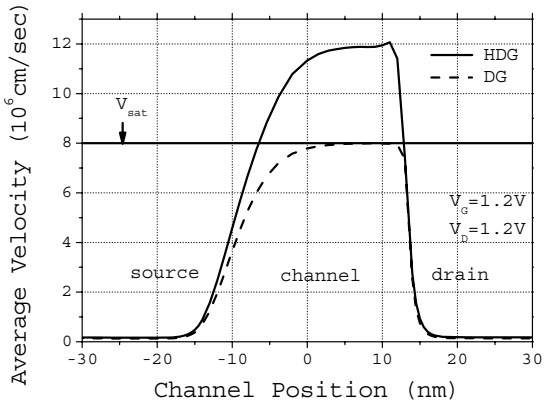


Fig. 8. Comparison of the average electron velocity in the channel between the DG and HDG models when $V_{\mathrm{G}}$ and $V_{\mathrm{D}}$ are 1.2V.

effect. We applied our model to the 25nm NMOSFET device, which is in the limit of the bulk MOSFET. The simulation results show that the quantum effect and the nonlocal transport effect can change the device characteristics about 20-30%. The simulation time is increased about 2–4 times compared with the semiclassical models, which is tolerable.

## ACKNOWLEDGMENT

The authors appreciate the support of the *National Research Laboratory Project of the Ministry of Science and Technology* and the *Brain Korea 21 Project*.

## REFERENCES

[1] S. Selberherr, *Analysis and Simulation of Semiconductor Devices*, pp. 127–148, Wien, Austria: Springer-Verlag, 1984.

[2] W. S. Choi, J. G. Ahn, Y. J. Park, H. S. Min, and C. G. Hwang, *IEEE Trans. on CAD*, vol. 13, no. 7, pp. 899–908, July 1994.

[3] M. G. Ancona and H. F. Tiersten, Phys. Rev. B, vol. 35, no. 15, pp. 7959–7965, May 1987.

[4] D. K. Ferry, R. Akis, and D. Vasileska, *Proc. of IEDM*, pp. 287–290, December 2000.

[5] J.-R. Zhou and D. K. Ferry, *IEEE Trans. on ED*, vol. 39, no. 3, pp. 473–478, March 1992.

[6] M. G. Ancona and G. J. Iafrate, Phys. Rev. B, vol. 39, no. 13, pp. 9536–9540, May 1989.

[7] D. Connelly, Z. Yu, and D. W. Yergeau, *IEEE Trans. on ED*, vol. 49, no. 4, pp. 619–626, April 2002.

[8] E. Lyumkis, R. Mickevicius, O. Penzin, B. Polsky, K. El Sayed, A. Wettstein, and W. Fichtner, *Proc. of SISPAD*, pp. 271–274, September 2002.

[9] Z. Yu, R. W. Dutton, and D. W. Yergeau, *Proc. of SISPAD*, pp. 1–9, September 2001.

[10] M. G. Ancona, Z. Yu, R. W. Dutton, P. J. V. Voorde, M. Cao, and D. Vook, *IEEE Trans. on ED*, vol. 47, no. 12, pp. 2310–2319, December 2000.

[11] J. R. Watling, A. R. Brown, A. Asenov, A. Svizhenko, and M. P. Anantram, *Proc. of SISPAD*, pp. 267–270, September 2002.

[12] I. Polishchuk and C. Hu, *Proc. of Symposium on VLSI Technology*, pp. 51–52, 2001.

[13] M. N. Darwish, J. L. Lentz, M. R. Pinto, P. M. Zeitzoff, T. J. Krutsick, H. H. Vuong, *IEEE Trans. on ED*, vol. 44, no. 9, pp. 1529–1538, September 1997.

[14] *MEDICI User's Manual*, Avant! Corp., Feb. 2001.

[15] G. Baccarani and M. Wordeman, *Solid-State Electronics*, vol. 28, no. 4, pp. 407–416, 1985.

[16] D. A. Antoniadis, I. J. Djomehri, K. M. Jackson, and S. Miller, *Well-Tempered Bulk-Si NMOSFET Device Home Page*, http://www-mtl.mit.edu/Well/, Microsystems Technology Laboratory, MIT.

[17] Y. Taur, C. H. Wann, and D. J. Frank, *Proc. of IEDM*, pp. 789–792, December 1998.

[18] Y. Taur et al., *Fundamentals of Modern VLSI Devices*, pp. 202–221, Cambridge University Press, 1998.

 